Measurement and control of optical nonlinearities in dispersive dielectric multilayers

GUAN GUI,[1] AMITAVA ADAK,[1] MANIKA DANDAPAT,[1] DANIEL CARLSON,[1] DREW MORRILL,[1] ALEXANDER GUGGENMOS,[2] HENRY KAPTEYN,[1,3] MARGARET MURNANE,[1] VLADIMIR PERVAK,[2,4] AND CHEN-TING LIAO[1,*]

[1]*JILA and Department of Physics, University of Colorado and NIST, 440 UCB, Boulder, Colorado 80309, USA*
[2]*UltraFast Innovations GmbH, Am Coulombwall 1, D-85748 Garching, Germany*
[3]*KMLabs Inc., 4775 Walnut Street, Suite 102, Boulder, Colorado 80301, USA*
[4]*Ludwig Maximilian University of Munich, Am Coulombwall 1, D-85748 Garching, Germany*
chenting.liao@colorado.edu

Abstract: Dispersive dielectric multilayer mirrors, high-dispersion chirped mirrors in particular, are widely used in modern ultrafast optics to manipulate spectral chirps of ultrashort laser pulses. Dispersive mirrors are routinely designed for dispersion compensation in ultrafast lasers and are assumed to be linear optical components. In this work, we report the experimental characterization of an unexpectedly strong nonlinear response in these chirped mirrors. At modest peak intensities <2 TW/cm^2—well below the known laser-induced damage threshold of these dielectric structures—we observed a strong reflectivity decrease, local heating, transient spectral modifications, and time-dependent absorption of the incident pulse. Through computational analysis, we found that the incident laser field can be enhanced by an order of magnitude in the dielectric layers of the structure. The field enhancement leads to a wavelength-dependent nonlinear absorption, that shows no signs of cumulative damage before catastrophic failure. The nonlinear absorption is not a simply two-photon process but instead is likely mediated by defects that facilitate two-photon absorption. To mitigate this issue, we designed and fabricated a dispersive multilayer design that strategically suppresses the field enhancement in the high-index layers, shifting the high-field regions to the larger-bandgap, low-index layers. This strategy significantly increases the maximum peak intensity that the mirror can sustain. However, our finding of an onset of nonlinear absorption even at 'modest' fluence and peak intensity has significant implications for numerous past published experimental works employing dispersive mirrors. Additionally, our results will guide future ultrafast experimental work and ultrafast laser design.

1. Introduction

Dispersive mirrors are widely used in ultrafast optics to manage the dispersion of broadband and ultrashort laser pulses. A dispersive mirror is a multilayer dielectric stack of alternative high and low refractive index materials with a controlled variation in thickness that results in a wavelength-dependent group delay. Group delay dispersion (GDD), third-order dispersion (TOD), and other higher order dispersions can be manipulated based on the wavelength-dependence of optical path length. A chirped mirror (CM) is a kind of dielectric dispersive mirror with a gradual change of layer thickness to achieve high-dispersion in broadband. CMs require extremely precise tolerances on layer thickness variation, typically resulting in some uncontrolled variation in this chirp imparted by the mirror. First introduced in the 1990s, CMs are useful in ultrafast optics for dispersion management [1], c.f., a recent comprehensive review [2]. One standout advantage of CMs, in comparison with alternative dispersive components such as prisms and

gratings, is that CMs provide dispersion control over a very broad spectral range without adding significant additional material in the beam path that could lead to nonlinear pulse distortions. CMs also introduce little to no spatial chirp, pulse front tilt, or wavefront distortion, simplifying the implementation of dispersion control. For these reasons, CM's have been used extensively in areas such as attosecond science [3,4], tabletop coherent extreme ultraviolet (EUV) and X-ray light sources [5,6], ultrafast laser modelocked oscillators [7], and optical waveform synthesis [3,8,9].

Another apparent advantage of using a CM is its high energy handling capability. As a reflective optical component with a nominal laser-induced damage threshold (LIDT) in the range of ∼200–350 mJ/cm^2 [10], they appear to be an excellent choice for dispersion compensation for high-energy pulses in the few-cycle range. However, it has recently been realized that nonlinear laser-material interactions in CMs can be problematic even though the interaction lengths are in microns. It was recently found that CMs for dispersion compensation in the ultraviolet (UV) spectral range is simply not usable at high power due to nonlinear effects enhanced by the higher UV photon energy [11]. These unwanted effects include nonlinear refraction and two-photon absorption.

In this work, we surprisingly identified similar nonlinear effects in CMs even when using near infrared (NIR) lasers with moderate laser fluence well below the LIDT. We show that these nonlinearities relate to the incident peak intensity, not the laser fluence, and do not result in damage to the mirror even in the long term. Thus, simple measurements of LIDT as defined by the current ISO standard (ISO 21254) are not sufficient for characterization and reliable use. To the best of our knowledge, this is the first report on such transient nonlinear effects of CMs in the most commonly used 800 nm spectral range. Our finding was unexpected since CMs have been used in high intensity ultrafast lasers for more than two decades, making this potentially a pervasive problem in the interpretation of past experimental work.

In this work, we experimentally characterized these nonlinear effects, measuring the peak intensity dependent mirror reflectance and the resultant pulse duration and beam profile after reflection. Strong local heating of the mirror surfaces even at moderate peak intensity is evident from thermal images of the CMs, providing a reliable way to diagnose and avoid this issue and its associated problems. To identify the mechanism behind this phenomenon, we conducted ultrafast pump-probe measurements capturing the transient changes in optical reflectance as well as spectral modifications from the CMs.

We also simulated the propagation of laser fields in the multilayer dielectric stacks. These simulations show order-of-magnitude scale field enhancements, resulting in the observed nonlinearities, especially when the enhancement coincides with the high-index layers. This insight suggested a revision of the dielectric stack design to alleviate nonlinear problems. Our mitigation approach includes reducing the use of high-index materials and placing the high fields inside the low-index layers to the extent possible. Experimental tests of these newly designed CMs confirmed that these mitigation strategies result in a significantly increased intensity capability without nonlinearities.

The mirror nonlinear response can also be useful in some applications. To illustrate this point, we demonstrated using the CM as a nonlinear optical limiter to spatially shape a moderately intense NIR beam, converting the Gaussian beam profile into a more flat-top beam without significantly affecting the pulse duration.

2. Experiment

A schematic of our experimental setup is shown in Fig. 1(a). Initially, we investigated high-dispersion mirrors HD58 and HD1631 designs from UltraFast Innovations GmbH. Our Ti:sapphire laser amplifier (Red Dragon, KM Labs Inc) delivers pulses of energy up to 16 mJ at 1 kHz repetition rate with a nominal pulse duration of ∼30 fs at ∼790 nm. For pump-probe experiments,

a 90/10 beamsplitter is used to pick-off a probe beam. The mirrors we studied here consist of Ta$_2$O$_5$ (n = 2.0957 at 800 nm) /SiO$_2$ (n = 1.4533 at 800 nm) multilayer dielectric stacks. The layer sequences for HD58 and HD1631 are shown in Figs. 1(b) and 1(c). Note these mirrors were never permanently damaged even with the highest incident laser peak intensity used in our experiments.
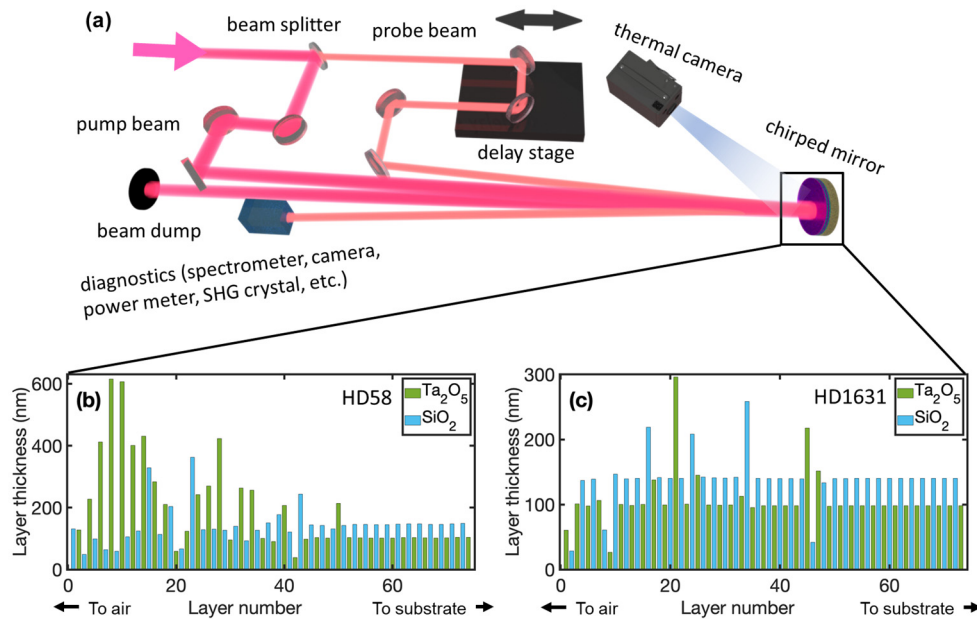

Fig. 1. (a) Sketch of experimental setup. Various diagnostic setups, including a power meter, a spectrometer, a beam profiler, a frequency-resolved optical gating (FROG) setup, and thermal and visible cameras were used to characterize both the reflected beam and the mirror. A pump-probe setup monitored the time-resolved reflectance of a weak probe beam following a string pump beam. (b, c) Layer sequences for the high-dispersion HD58 and HD1631 chirped mirrors we evaluated.

Figure 2 shows the power loss from the mirror on reflection, as a function of incident peak intensity, where the peak intensity was varied by adjusting the incident power. The nominal reflectance of both CMs at low intensity was 99.5% within the design wavelength range of ~770–830 nm, at 5° angle of incidence for p-polarization. Figures 2(a) and 2(b) show the total reflectance of both HD58 and HD1631 mirrors as a function of incident laser peak intensity, averaged over the laser beam size. A power loss of up to ~16% was observed in HD58 at ~5.89 ± 0.52 TW/cm^2 and up to 8.9% for HD1631 at ~3.89 ± 0.35 TW/cm^2. Note that the maximal loss here is beam size averaged, and the local maximal reflectance reduction was > 20%. Blue and red data points indicate the increasing and decreasing laser peak intensities during the measurement, indicating no hysteresis or irreversibly damage. None of this power loss was observed to be light transmitted through the mirror—the power is fully absorbed in the multilayer structure This loss is plotted on a log-log scale in Figs. 2(b) and 2(e), along with power-law fits that clearly indicate an absorption quadratic with incident average power, indicating a two-photon absorption (TPA) process. Although neither the bandgap of Ta$_2$O$_5$ (~4.2 eV) nor of SiO$_2$ (~7.5 eV) supports TPA at ~790 nm (~1.57 eV), potential defect states in the forbidden bands of Ta$_2$O$_5$ could allow for TPA [11]. We simulated TPA, three-photon absorption, and four-photon absorption processes in pure materials, however, none of these simulations can reproduce the

peak intensity dependent power losses we observed experimentally, suggesting that complex, likely defect-mediated processes, are involved [12].
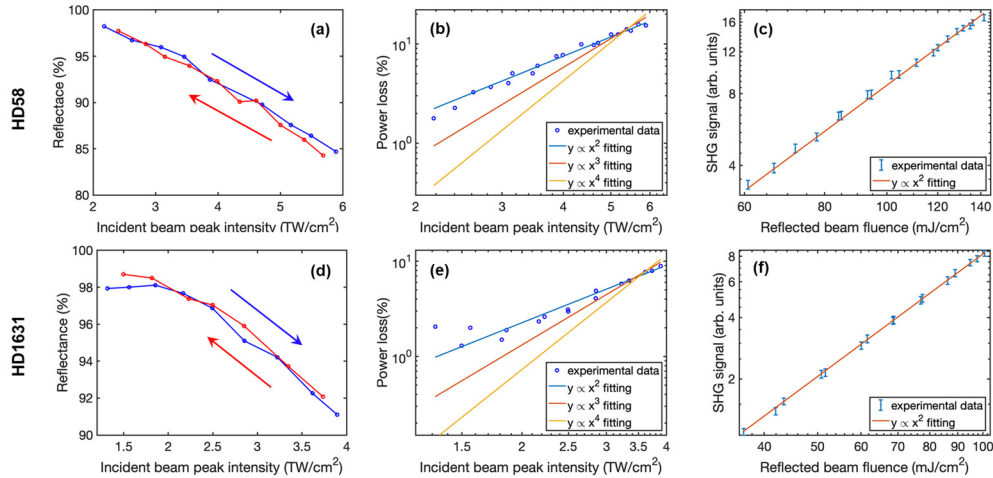

Fig. 2. Intensity-dependent performance of high-dispersion HD58 (top graphs) and HD1631 (bottom) chirped mirrors. (a, d) Measured reflectance as a function of incident laser peak intensity, averaged over the laser beam size. These data show a clear reduction in reflectance beyond $\sim 2 \pm 0.2$ TW/cm^2. Blue (red) data points and the arrow indicates the increasing (decreasing) peak intensities when taking the measurements, verifying a the reproducible and fully reversible effect. (b, e) Power loss on reflection as a function of peak intensity on a log-log scale, along with power-law fits showing that the absorption fits a quadratic power law. (c, f) SHG signal generated with the reflected laser beam, as a function of the reflected laser fluence on a log-log plot. These SHG signal fits a quadratic power law, indicating the duration of the reflected pulses was not significantly changed by the strong nonlinear absorption.

Nonlinear absorption has the potential to reshape an ultrashort pulse, and furthermore, absorption-induced heating alters the mirrors chirp characteristics, by slightly shifting the working range. It is mainly the imaginary part of refractive index changes, thus there are no direct changes to GDD. Thus, to further characterize the reflected beam, we measured the SHG signal generated by that beam, using a BBO crystal. Figures 2(c) and 2(f) show this SHG signal, as a function of fluence for a beam reflected with optimized peak intensity. These data can also be fit well by a quadratic power-law function, indicating that the peak intensity is proportional to the fluence. This implies that the duration of the reflected pulses is not significantly altered by the nonlinear absorption.

To distinguish a peak intensity effects from fluence-related effects, we varied the incoming chirp of the pulse using the compression gratings, stretching the pulse to up to ~1 ps to reduce the peak intensity. These data show that the absorption is entirely related to the peak intensity, not the average fluence. This is further evident using thermal camera (E5, FLIR Systems, Inc.) images. Figure 3 shows a series of images as the pulse chirp is changed at constant fluence, after ~1 minute of illumination to allow the mirror to reach an equilibrium temperature. The crosshairs on the images correspond to the position of the highest temperature, with the temperature reading shown on the top-left corner. The black circles on the images mark the mirror position for clarity. The temperature can easily reach at least ~100 °C when illuminated by short pulses, with the temperature profile following the Gaussian profile of the incident laser beam. With long pulses, the temperature remains close to the room temperature. This behavior can be observed on both

CM designs, and clearly indicates a peak intensity-dependent effect. The thermal camera provides an easy way to diagnose the potential nonlinear effects and their associated problems. More detailed thermal images and their corresponding visible images can be found in the supplementary material Fig. S1.
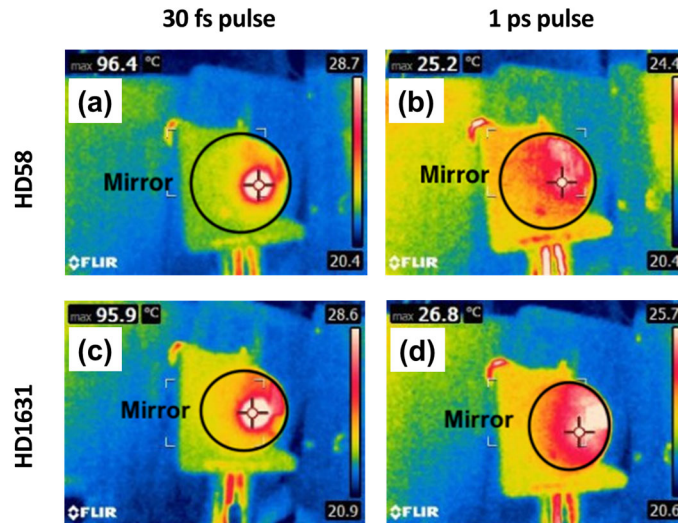

Fig. 3. Thermal images of HD58 (top) and HD1631 (bottom) when illuminated by the same laser fluence ($\sim$80.2 mJ/cm^2) with two different peak intensities by changing the pulse duration from 30 fs (a, c) to 1 ps (b, d). Localized heating up to $\sim$100 °C can be observed at the center of the laser beam from both types of chirped mirrors (a, c) at moderately strong laser peak intensity of $\sim$2.5 $\pm$ 0.2 TW/cm^2. At a lower laser peak ($\sim$0.08 TW/cm^2), no significant heating above the ambient room temperature was observed (b, d). The black circles on the images mark the mirror position for clarity.

In addition to static characterization, we also conducted time-resolved pump-probe measurements. Here we used a pump pulse at a moderately strong peak intensity of 2.5 $\pm$ 0.2 TW/cm^2 (fluence $\sim$80.2 mJ/cm^2) and a probe pulse at a low peak intensity < 10 GW/cm^2 (fluence $\sim$0.3 mJ/cm^2). Both the pump and probe beams are linearly polarized and are at $\sim$5° AOI. The plane of incidence for the pump and the probe beams are vertical and horizontal, respectively, to isolate the probe beams while maintaining the design AOI of the mirrors. We also varied the probe beam polarization direction using a half-wave plate but did not observe any polarization dependence, as expected for the near-normal AOI. The $\sim$1 mm probe beam diameter was much smaller than the 7 mm pump beam and positioned at the center of the pump beam, where nonlinear absorption was strongest. Figure 4 shows the time-resolved power loss of the probe beam. Both designs of the CMs, HD58 (blue circle) and HD1631 (red square), show a transient and large power loss within $\sim$1 ps time scale, followed by a slow $\sim$10's of ps recovery. The decay time constants of the two designs of CMs differ.

The measurement shown in Fig. 4 can be best understood through a two-stage process. First, multiphoton absorption and free electron formation lead to a sudden power loss (i.e. increase in absorption). Although our CMs consist of wide bandgap dielectric materials ($\sim$4.2 eV for Ta$_2$O$_5$; $\sim$7.5 eV for SiO$_2$) [11], electrons in the valence band can be photoexcited to the conduction band by defect-mediated multiphoton absorption. Because of its smaller bandgap, this absorption will be strongest in the Ta$_2$O$_5$ layers. Due to the presence of free electrons in the conduction band after photoexcitation, the dielectric layers become more absorptive to the probe pulse through inverse

bremsstrahlung absorption [13]. The slow recovery is related to the formation of long-lived self-trapped exciton states. At a few picosecond range, free electrons in the conduction band can be trapped to local lattice sites, leading to the formation of self-trapped excitons, which are transient defect states between the valence band and the conduction band in Ta_2O_5 [14,15]. The lifetime of self-trapped excitons in Ta_2O_5 can exceed 100 ps at room temperature [13], which could explain the non-zero power loss even after 80 ps.

In addition to the transient power loss, we also investigated the transient spectrum change for the probe beam as shown in Figs. 5(a) and 5(b). The transient spectrum change of the probe beam is defined as $(I_{PumpOn}(\lambda, t) - I_{PumpOff}(\lambda)) / I_{PumpOff}(\lambda)$, where I_{PumpOn} is the spectrum of the probe beam in the presence of a delayed pump pulse at a peak intensity of 2.5 ± 0.5 TW/cm^2, and $I_{PumpOff}$ is the spectrum of the probe beam in the absence of a pump pulse. As we can see the two mirror designs, HD58 and HD1631, show the strongest spectral absorption around 810 nm, which is red-shifted by ~20 nm with respect to the peak spectrum of the incident laser. The absorption at ~ 810 nm can go as high as ~35%. The same red shifting is also observed on the side panels of Figs. 5(a) and 5(b), which shows the probe spectrum at representative pump-probe delays of 0 ps, 4 ps, and 24 ps.
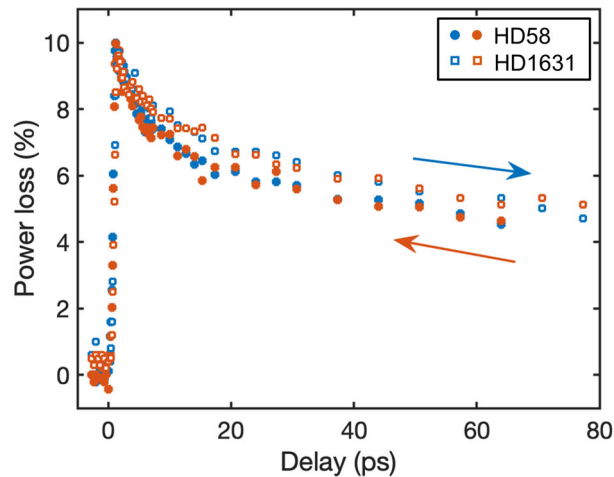

Fig. 4. Time-resolved power loss of the probe beam due to pump beam induced transient reflectance change of the CMs. Blue and red symbols are for HD58 and HD1631 designs, respectively. Ascending (descending) delay means the data are acquired with ascending (descending) delays in the delay line, where positive delay implies the pump pulse arrives at the CM before the probe pulse.

Despite the significant spectral modification of the probe pulse, we found its impact on the pulse duration of the probe to be minimal. Figure 5(c) shows the pulse duration measured by an SHG frequency-resolved optical gating (FROG) setup. At each delay, the pulse duration was measured by averaging several reconstructed pulse durations. We observed that the FROG reconstructed probe pulse durations change by less than ~2 fs on average at all delays. We also calculated the Fourier-transform-limited (FTL) pulse of the probe beam, assuming a flat phase from the measured spectra at different delays. Figure 5(d) shows the FTL pulses at two representative delays of 0 ps and 4 ps, where we found that these FTL pulses have very similar pulse durations, confirming our FROG measurements at different delays. The result of the minimal change in pulse duration of both probe beam, as shown here, and pump beam, as shown in Fig. 2(e), Fig. 2(f) indicates that the mirrors do not significantly distort pulses in this range of duration. It confirms that we only have changes in the imaginary part of the refractive index. If
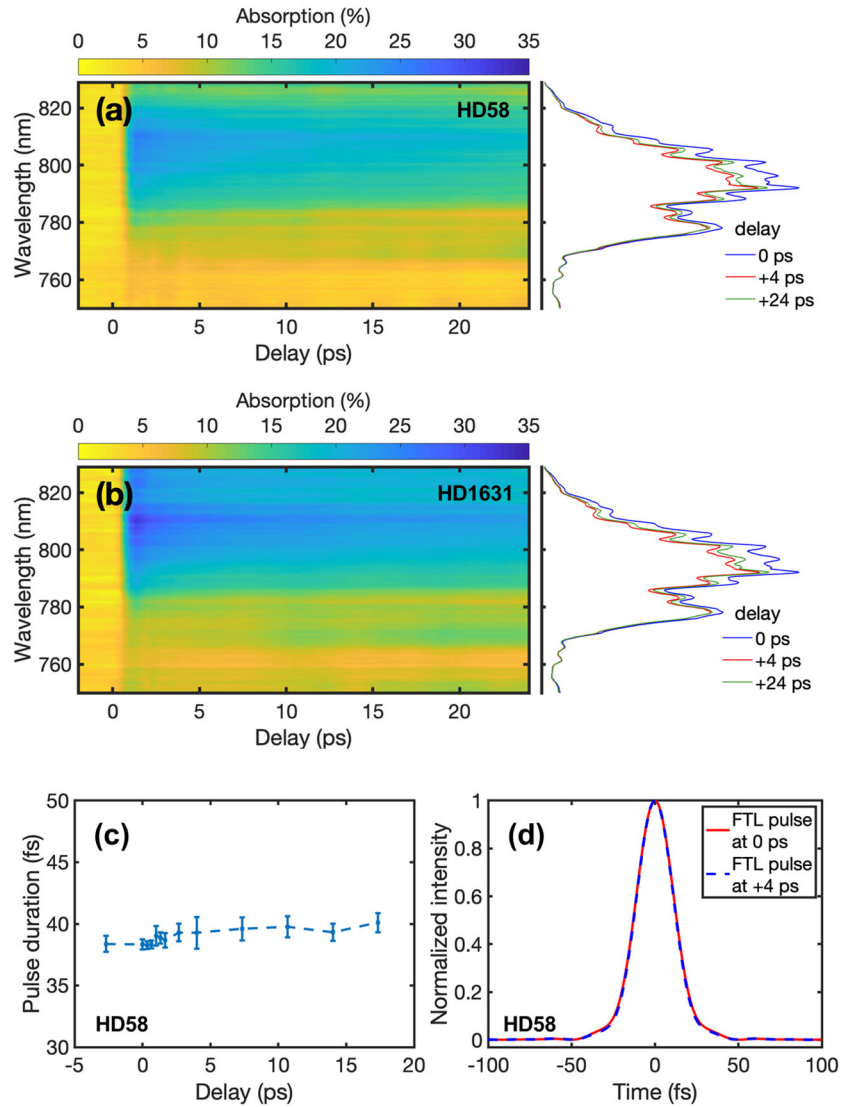
Fig. 5. Time-resolved spectral change, i.e., transient absorption spectrogram, of the probe beam in the presence of a pump beam for (a) HD58 and (b) HD1631 mirrors. (c) Probe beam pulse duration, measured with SHG FROG, as a function of pump-probe delay for the CM HD58. Minimal changes are observed. (d) Fourier-transform-limited (FTL) pulses calculated from the spectra of probe beam from HD58 at 0 and +4 ps delay.

changes would happen in the real part of the refractive index we would have strong changes in GDD.

Our findings are surprising in that a large body of experimental work has used pulse compression with dispersive mirrors, and much of this work up or down-converts light to other spectral ranges such as terahertz, mid-infrared, EUV, soft X-ray using mJ-level pulse energies. The effect of the observed pulse distortions is likely to be greater for even-shorter sub-10-fs pulses, but in the absence of recognition of this absorption phenomenon, these effects are completely uncharacterized in past work—and may have a non-negligible influence on results and conclusions. As a result, care must be taken when quantitatively interpreting such experimental results.

To better understand these effects, we calculated the electric field intensity in the dispersive multilayer stacks themselves using Optilayer software (Optilayer GmbH) [16]. The multilayer structure used in the simulation is based on the design data as in Fig. 1(b). Detailed information of the simulation can be found in the supplementary materials. The results are shown in Fig. 6 for HD58. Figure 6(a) shows the wavelength-dependent field distribution across the multilayer. This calculation assumed a pulse with a flat spectrum spanning 700–900 nm for simplicity, and the field in the multilayer is normalized to the incident field shown in the color bar. As expected, longer wavelengths propagate deeper to impart a negative chirp on the reflected pulse. Furthermore, the longer wavelengths see a larger field enhancement ratio.
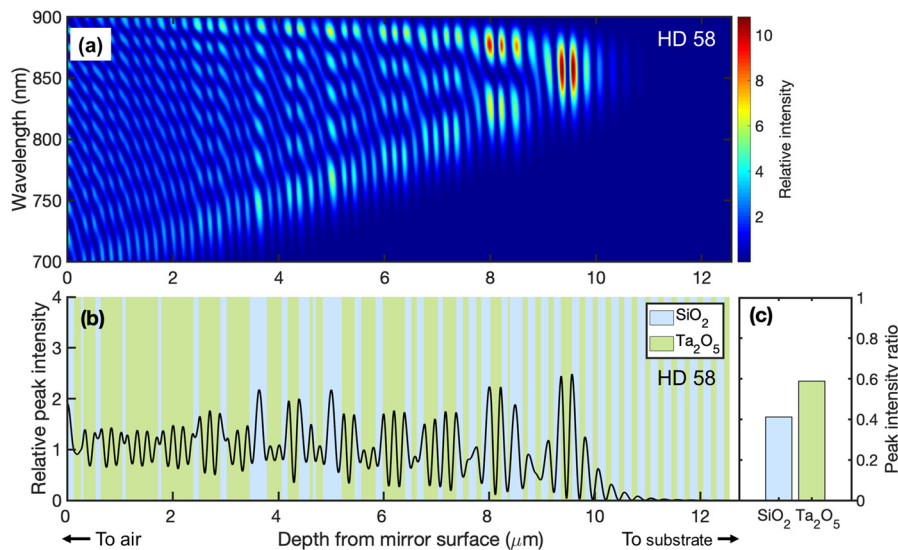

Fig. 6. (a) Theoretical simulations of the spectral intensity distribution in HD58 dispersive multilayer with a flat top spectrum input. (b, c) Theoretical simulations of integrated electric field intensity in HD58 dispersive multilayer stacks with an experimental spectrum input from Ti:sapphire laser. The right figures show the volume integrated peak intensity ratio between Ta_2O_5 and SiO_2.

Figure 6(b) shows the spectrum-integrated electric field distribution for HD58 in the case where the incident pulse has a spectrum corresponding to that of a typical Ti:sapphire laser amplifier system. Here we observe that the field enhancement happens mostly in the Ta_2O_5 layers. Figure 6(c) shows the volume integrated field intensity ratio of SiO_2 and Ta_2O_5, namely, the horizontal summation of Fig. 6(c) but with two material separated. As we can see, the field enhancement in Ta_2O_5 is the dominant one that contributes to the nonlinear effects. We simulated CM HD1631 as well, as shown in Fig. S8. All of these supplementary figures demonstrate similar nonlinear phenomena and support the same general conclusions.

Based on this understanding, a new multilayer dielectric stack high-dispersion HD1858 chirped mirror was designed, using custom made option in Optilayer software [16]. The layer sequence data for this HD1858 is shown in Fig. 7(a). Comparing to the original design of HD58 [Fig. 1(b)], this design uses less Ta_2O_5. The experimental thermal image of this new HD1858 mirror, as shown in Fig. 7(b), indicates that the peak temperature increase is much less for the same fluence and peak intensity used with the previous designs. From the field enhancement simulation of the HD1858 in Fig. 7(c), we can see that the field enhancement in Ta_2O_5 is much weaker by strategically placing the high field inside the lower-index material SiO_2 to suppress the intensity enhancement ratio. This strategy is further evident by plotting the volume integrated peak intensity ratio between Ta_2O_5 and SiO_2 as in Fig. 7(d). More detailed experimental characterization as well as simulations can be found in the supplementary figures Fig. S8 here we measured the peak intensity dependent reflectance, the SHG signal dependence after reflection, and their temperature profiles. The group delay of this new mirror design configuration (HD1858) is measured and compared with original mirrors (HD58 and HD1631), as shown in the supplementary material Fig. S2.
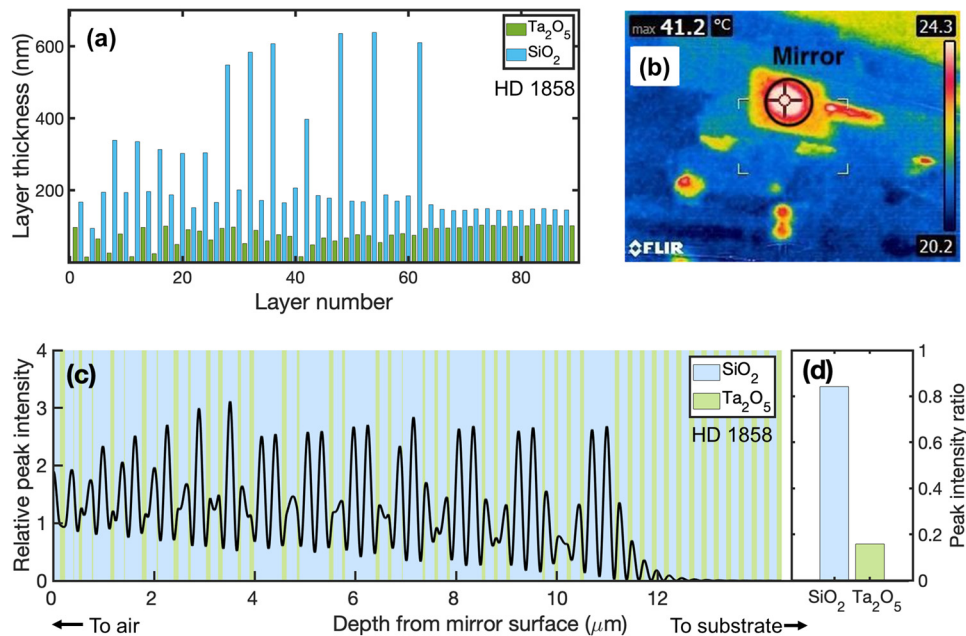

Fig. 7. (a) The layer sequence of the new high-dispersion HD1858 chirped mirror we designed and fabricated. (b) A thermal image of the HD1858 mirror when illuminated by 30 fs pulse. (c, d) Theoretical simulations of integrated electric field intensity in HD1858 dispersive multilayer with an experimental spectrum input from Ti:sapphire laser. The right figures show the volume integrated peak intensity ratio between Ta_2O_5 and SiO_2.

Moreover, we numerically investigated the feasibility and the influence of using these to compress pre-chirped pulses in the supplementary material in Fig. S4-6. These calculations make it possible to determine the loss in peak intensity that results from ripples in the dispersion compensation. In understanding the overall efficiency with which dispersive mirror can be used for compression of high-energy, high peak-intensity pulses, the nonlinear energy loss, the spectral distortion, and the ripples in the dispersion compensation all degrade the focusable peak intensity achievable.
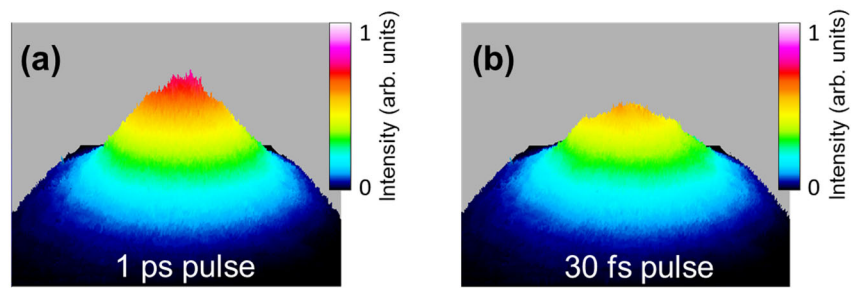
Fig. 8. **Use of CMs for nonlinear beam shaping of a Gaussian beam, (a), to a more flat-top super-Gaussian beam shape, (b).** By increasing the laser peak intensity, shortening the pulse duration, adding more bounces from one or more CM's, the amount of the profile flattening can be controlled. Here the experimentally measured flat-top beam profile is achieved by an HD58 CM. Field of view for the camera is 11.3×11.3 mm.

However, for some applications, this nonlinear absorption could be used to advantage. Figure 8 shows how these CM's can be used as a flat-top (or top-hat) beam shaper. Flat-top and super-Gaussian beams are useful for shaping the focal spot for HHG for EUV generation to avoid ionization depletion [17,18], constructing Ponderomotive optical traps for energetic electron beams [19,20], accelerating charged protons [21], and building next-generation petawatt or exawatt laser systems. When illuminating a femtosecond pulse with ~2.5 TW/cm^2 peak intensity on an HD58 CM over multiple bounces, we can suppress the intensity of the central beam profile, as shown in Fig. 8. Note that this peak intensity can be easily achieved even with a tightly focused Ti:sapphire laser oscillator. This reshaping also must occur to some extent in the spectral domain since the CM attenuates most-strongly the region of the spectrum the corresponds to a convolution of the incident spectrum and the field enhancement. This could provide an alternative route to counteracting a gain narrowing in a downstream amplification process, including optical parametric amplification and Raman amplification. However, either of these processes does introduce a spatio-spectral and therefore a spatio-temporal coupling that must be carefully considered for the most demanding applications.

3. Conclusion

In this work, we report the first observation of transient nonlinear effects in dispersive mirrors in the commonly used 800 nm spectral range. Such nonlinear effects can be observed at peak intensity as low as a few TW/cm^2, an order of magnitude below the known damage threshold. These effects are peak intensity, not fluence, dependent. Time resolved observations indicate a defect-mediated direct multiphoton absorption, creating long-lived free carriers in the multilayer stack. This nonlinearity can be severe, >20% absorption, and alters both the spatial and the spectral profile of the light reflected from the mirror, with a minimal effect on the duration of the reflected ultrashort pulses. This nonlinearity is completely reversible and reproducible, with no permanent mirror damage. By taking nonlinear absorption into account in the layer stack design, these nonlinear effects can be suppressed by >~2x, substantially increasing the pulse energy handling characteristics of the mirror. Our findings may have a significant impact on the interpretation of past experimental work, especially on time-resolved experiments that could be affected by the long relaxation time of the nonlinear response. In other cases, these nonlinear effects can be used or engineered for applications including direct beam shaping of ultrafast laser pulses in the spatial and spectral/temporal domains.

Disclosures. The authors declare that there are no conflicts of interest related to this article.

Supplemental document. See Supplement 1 for supporting content.

References

1. R. Szipöcs, C. Spielmann, F. Krausz, and K. Ferencz, "Chirped multilayer coatings for broadband dispersion control in femtosecond lasers," Opt. Lett. **19**(3), 201 (1994).
2. O. Razskazovskaya, F. Krausz, and V. Pervak, "Multilayer coatings for femto- and attosecond technology," Optica **4**(1), 129–138 (2017).
3. F. K. E. Goulielmakis, V. S. Yakovlev, A. L. Cavalieri, M. Uiberacker, V. Pervak, A. Apolonski, R. Kienberger, and U. Kleineberg, "Attosecond Control and Measurement: Lightwave Electronics," Science **317**(5839), 769–775 (2007).
4. X. Feng, S. Gilbertson, H. Mashiko, H. Wang, S. D. Khan, M. Chini, Y. Wu, K. Zhao, and Z. Chang, "Generation of Isolated Attosecond Pulses with 20 to 28 Femtosecond Lasers," Phys. Rev. Lett. **103**(18), 183901 (2009).
5. T. Popmintchev, M.-C. Chen, P. Arpin, M. M. Murnane, and H. C. Kapteyn, "The attosecond nonlinear optics of bright coherent X-ray generation," Nat. Photonics **4**(12), 822–832 (2010).
6. T. Popmintchev, M.-C. Chen, D. Popmintchev, P. Arpin, S. Brown, S. Alisauskas, G. Andriukaitis, T. Balciunas, O. D. Mucke, A. Pugzlys, A. Baltuska, B. Shim, S. E. Schrauth, A. Gaeta, C. Hernandez-Garcia, L. Plaja, A. Becker, A. Jaron-Becker, M. M. Murnane, and H. C. Kapteyn, "Bright Coherent Ultrahigh Harmonics in the keV X-ray Regime from Mid-Infrared Femtosecond Lasers," Science **336**(6086), 1287–1291 (2012).
7. J. P. Zhou, G. Taft, C. P. Huang, M. M. Murnane, H. C. Kapteyn, and I. P. Christov, "Pulse Evolution in a Broad-Bandwidth Ti-Sapphire Laser," Opt. Lett. **19**(15), 1149–1151 (1994).
8. S.-H. Chia, O. D. Mücke, F. X. Kärtner, G. M. Rossi, S. Fang, and G. Cirmi, "Two-octave-spanning dispersion-controlled precision optics for sub-optical-cycle waveform synthesizers," Optica **1**(5), 315 (2014).
9. M. T. Hassan, A. Wirth, I. Grguraš, A. Moulet, T. T. Luu, J. Gagnon, V. Pervak, and E. Goulielmakis, "Invited Article: Attosecond photonics: Synthesis and control of light transients," Rev. Sci. Instrum. **83**(11), 111301 (2012).
10. I. B. Angelov, S. A. Trushin, V. Pervak, S. Karsch, Z. Major, A. von Conta, and F. Krausz, "Investigation of the laser-induced damage of dispersive coatings," Laser-Induced Damage Opt. Mater. **8190**, 81900B (2011).
11. O. Razskazovskaya, T. T. Luu, M. Trubetskov, E. Goulielmakis, and V. Pervak, "Nonlinear absorbance in dielectric multilayers," Optica **2**(9), 803 (2015).
12. D. Ristau, M. Jupé, and K. Starke, "Laser damage thresholds of optical coatings," Thin Solid Films **518**(5), 1607–1613 (2009).
13. D. Grojo, M. Gertsvolf, S. Lei, T. Barillot, D. M. Rayner, and P. B. Corkum, "Exciton-seeded multiphoton ionization in bulk SiO2," Phys. Rev. B 3–6 (2010).
14. J. Zeller, W. Rudolph, M. Mero, and A. J. Sabbah, "Femtosecond dynamics of dielectric films in the pre-ablation regime," Appl. Phys. A: Mater. Sci. Process. **81**(2), 317–324 (2005).
15. P. Martin, S. Guizard, P. Daguzan, and G. Petite, "Subpicosecond study of carrier trapping dynamics in wide-band-gap crystals," Phys. Rev. B 55, (1997).
16. M. Trubetskov and A. Tikhonravov, Optilayer Software [software] (2019), https://www.optilayer.com
17. H. G. M. E S Toma, Ph Antoine, and A de Bohan, "Resonance-enhanced high-harmonic generation," J. Phys. B: At., Mol. Opt. Phys. **32**(24), 5843 (1999).
18. W. Boutu, T. Auguste, O. Boyko, I. Sola, P. Balcou, L. Binazon, O. Gobert, H. Merdji, C. Valentin, E. Constant, E. Mével, and B. Carré, "High-order-harmonic generation in gas with a flat-top laser beam," Phys. Rev. A: At., Mol., Opt. Phys. **84**(6), 063406 (2011).
19. J. L. Chaloupka, Y. Fisher, T. J. Kessler, and D. D. Meyerhofer, "Single-beam, ponderomotive-optical trap for free electrons and neutral atoms," Opt. Lett. **22**(13), 1021 (1997).
20. W. P. Leemans, A. J. Gonsalves, H. S. Mao, K. Nakamura, C. Benedetti, C. B. Schroeder, C. Tóth, J. Daniels, D. E. Mittelberger, S. S. Bulanov, J. L. Vay, C. G. R. Geddes, and E. Esarey, "Multi-Gev electron beams from capillary-discharge-guided subpetawatt laser pulses in the self-trapping regime," Phys. Rev. Lett. **113**(24), 245002 (2014).
21. S. S. Bulanov, A. Brantov, V. Y. Bychenkov, V. Chvykov, G. Kalinchenko, T. Matsuoka, P. Rousseau, S. Reed, V. Yanovsky, D. W. Litzenberg, K. Krushelnick, and A. Maksimchuk, "Accelerating monoenergetic protons from ultrathin foils by flat-top laser pulses in the directed-Coulomb-explosion regime," Phys. Rev. E: Stat., Nonlinear, Soft Matter Phys. **78**(2), 026412 (2008).